Characterization of entrained air voids in cement paste with scattered ultrasound

Wonsiri Punurai[a], Jacek Jarzynski[b], Jianmin Qu[b], Kimberly E. Kurtis[a],
Laurence J. Jacobs[a,b,*]

[a]School of Civil and Environmental Engineering, Georgia Institute of Technology, Atlanta, GA 30332–0355, USA
[b]G.W. Woodruff School of Mechanical Engineering, Georgia Institute of Technology, Atlanta, GA 30332–0405, USA

Abstract

This research develops a technique that uses the attenuation of ultrasonic waves to characterize the average size and volume fraction of entrained air voids in hardened cement paste. Quantitative knowledge of entrained air void size and distribution helps ensure that an adequate design strength is developed, while maintaining resistance to freeze-thaw damage in cement-based materials. Ultrasonic attenuation coefficients obtained from pulse-burst signals are measured in the frequency range of 500 kHz–5 MHz. From these parameters, the average size and the volume fraction of the entrained air voids are determined using a combination of an ultrasonic scattering model and an inversion algorithm. Experiments are performed on specimens produced with and without entrained air voids. There is a good agreement between the model prediction and the experiments in these systems that contained < 10% by volume of entrained air voids.

1. Introduction

When concrete is expected to be exposed to cycles of freezing and thawing in service, chemical air-entraining agents are typically used to impart a system of well-dispersed voids (0.05–1.25 mm diameter, up to about 10%) which serve to protect the concrete from damage resulting from expansion of freezing water [1]. However, too great an air content can unnecessarily decrease compressive strength of the concrete. For each 1% of added air entrainment, there is approximately 3% to 5% loss in the compressive strength. When entrained air is high (7% and higher), entrained air voids congregate along the surfaces of aggregates, causing additional strength loss at the interface between the cement paste and aggregate. The air content in fresh concrete mixtures is typically measured soon after production using standard gravimetric [2], volumetric [3] or pressure [4] methods. However, the volume of entrained air can be affected by normal construction operations (e.g., placement, compaction vibration, finishing), and, as a result, measurements of air content in fresh concrete are not necessarily representative of the actual air content in situ. In addition, these standard methods are often cumbersome to perform and do not provide information regarding the size and distribution of the air voids.

In contrast, ultrasonic techniques (which use quantitative attenuation measurements) have the potential to provide in situ measurements of both air void size and volume fraction. Previous studies have been successful in relating ultrasonic attenuation with grain size and porosity in ceramic and metallic materials [5,6]. Ultrasonic waves have shown to be very effective in characterizing distributed voids in structural materials, with several well-accepted scattering models available in the literature

*Corresponding author. School of Civil and Environmental Engineering, Georgia Institute of Technology, Atlanta, GA 30332–0355, USA. Tel.: +1 404 894 2771; fax: +1 404 894 2278.

E-mail address: laurence.jacobs@ce.gatech.edu (L.J. Jacobs).

(e.g., [7–9]). Among them, the formalism in [8] and effective medium theory may be used when the wavelength is much greater than the size of the scatterers, while the diffusion approximation is valid for a wavelength much smaller than the size of scatterers. In the framework of resonance cavity scattering theory, Gaunaurd and Überall [10] extended the treatment of single scattering resonances presented by Waterman and Truell [11] into a multiple scattering formalism, which allows for the treatment of a low volume of the same size voids (on the same order as the wavelength) embedded in a viscoelastic matrix. An important aspect of these analytical models is that they directly provide the attenuation coefficients for long-itudinal and transverse waves; these attenuation coefficients can be directly measured in different materials. For example, Sayers et al. [12] investigate ultrasonic attenuation in porous media using the multiple scattering theory of [11]. Finally, Morochnik [13], Brauner and Beltzer [14], Biwa [15], and Kim [16] provide formulations for wave scattering in a viscoelastic matrix, and these results have been successfully applied to characterize various particle-reinforced polymer matrix composites.

A number of researchers have investigated ultrasonic wave propagation in cement-based materials; this is a challenging class of materials since their heterogeneous nature leads to complex wave behavior. Moreover, ultrasonic waves in cement-based materials are highly attenuated because: (i) the paste matrix is viscoelastic; and (ii) significant energy can be scattered by several types of inclusions including aggregate, air voids, and microcracks. Recent studies by Landis [17], Popovics et al. [18], and Jacobs and Owino [19] have investigated sources of attenuation losses in cement-based materials. Anugonda et al. [20], and Becker et al. [21] applied a statistical approach plus diffusion theory to cement-based materials to calculate diffusion and dissipation parameters (measures of attenuation). These studies can experimentally resolve the effect of different features of the microstructure on attenuation, but do not provide direct information about the size or volume fraction of the microstructure of interest.

The objective of the current research is to apply established ultrasonic scattering models and develop a procedure to measure average entrained air void size and volume fraction in in situ hydrated cement paste. This study considers a real, but simplified cement-based material, cement paste, which consists of Portland cement and water, but does not include any fine or coarse aggregates. Cement paste is the binding matrix of all cement-based materials, and a quantitative understanding of attenuation in this material is a critical step in the understanding of ultrasonic wave propagation in concrete components.

A theoretical model for attenuation behavior of long-itudinal waves is applied to a two component system composed of entrained air voids and viscoelastic cement paste matrix [15]. This model, which assumes only a single

size scatterer (assumes that all entrained air voids are the same size) and neglects any interaction between the scatterers (it is only valid for a relatively low volume fraction of entrained air voids) is used to demonstrate the influence of air void size and volume fraction on the attenuation coefficients. Next, attenuation experiments (in the frequency range of 500 kHz–5 MHz) are performed in cement paste specimens with and without entrained air voids. Finally, an inversion procedure is used to predict the average size and the volume fraction of the entrained air voids.

2. Theoretical modeling—forward problem

Cement grains react chemically with water to form hydration products. These products, any residual unhy-drated cement, and the intrinsic multiscale porosity forms a viscoelastic cement paste matrix. Fig. 1(a) shows a magnified digital image of a cement paste (only) specimen, while Fig. 1(b) shows a magnified digital image of a cement paste matrix cast with an air-entraining agent (cement
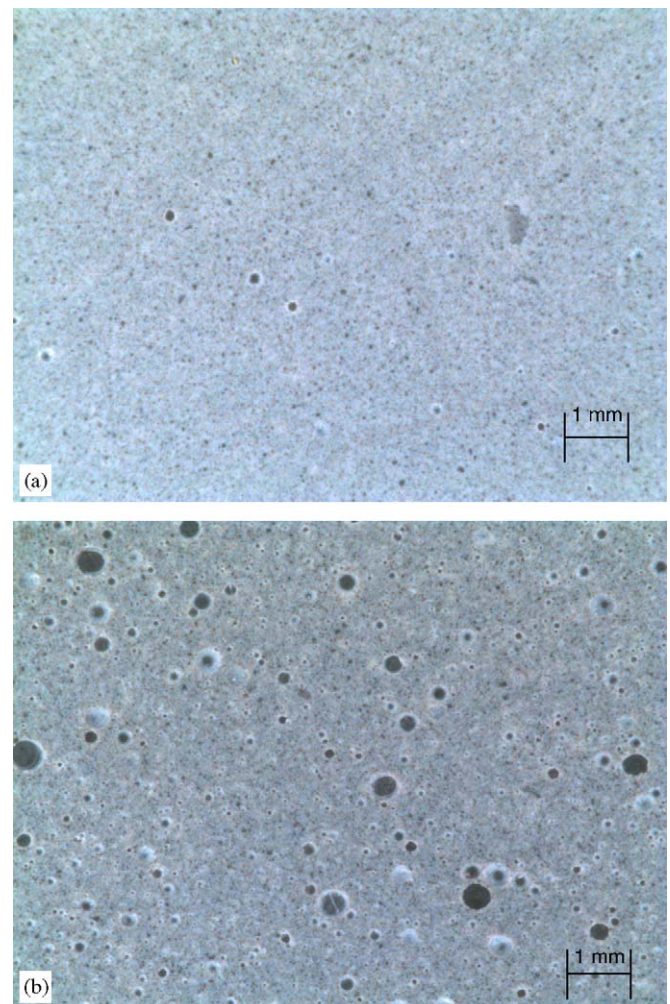

Fig. 1. Magnified digital images of the two specimens: (a) cement paste specimen; (b) entrained air specimen.

paste with entrained air voids). Details of the casting procedure for these two specimens are presented in Section 3. Note that the cement paste (only) specimen contains some intrinsic porosity that are not due to the air-entraining agent—these voids are clearly visible in Fig. 1(a).

Assume that the entrained air specimen shown in Fig. 1(b) is a two-component system—a cement paste matrix (which includes some intrinsic porosity) with a distribution of spherical air voids; these voids, then, are those produced by the addition of an air-entraining agent, typically a surfactant which produces well-spaced, spherical porosity within the matrix. A theoretical model for ultrasonic wave attenuation in such a two-component system is shown in Fig. 2—the model consists of (single sized) spherical entrained air voids of radius a embedded in an isotropic viscoelastic matrix. The total number of entrained air voids per unit volume of the system is denoted as, n_s and is related to the volume fraction, ϕ, by $\phi = \frac{4}{3}\pi a^3 n_s$. If this system is subjected to an incident time-harmonic plane wave, the energy loss rate of the combined scattering by the air voids and the viscoelastic absorption in the matrix can be estimated following [15]. This model is based on the assumption that there is no interaction between neighboring air voids, and that the scattering loss can be evaluated using the scattering cross section γ^{sca} of a single scatterer (entrained air void) in an infinite matrix. The absorption loss in the viscoelastic matrix is found to decrease in proportion to the volume fraction of the entrained air voids, so the total attenuation coefficient of this two component system is

$$\alpha = (1 - \phi)\alpha_a + \frac{1}{2}n_s\gamma^{\mathrm{sca}}, \tag{1}$$

where α_a is the absorption attenuation coefficient of the incident wave in the viscoelastic matrix (1/m or Neper/m) and γ^{sca} is the scattering cross section of a single spherical air entrained void (m²). The above expression implies that the total attenuation of this two component system is the addition of the two quantities—reduced absorption attenuation due to the presence of the entrained air voids
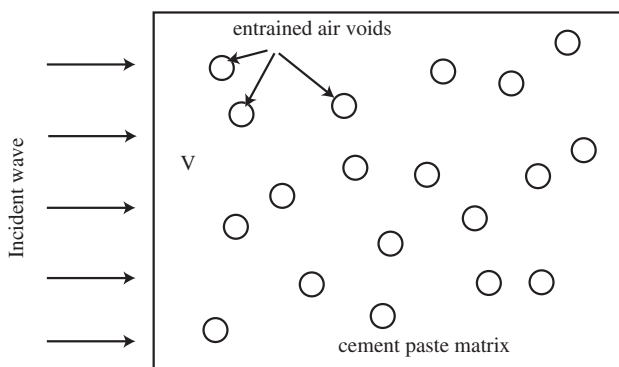
of volume fraction, ϕ, in the viscoelastic matrix, and the scattering attenuation due to the entrained air voids. This equation makes it possible to separate the calculated attenuation coefficient of ultrasonic waves in this two component system into: the absorption attenuation of the viscoelastic matrix (when the entrained air voids are absent); the entrained air void size; and the entrained air void volume fraction.

Eq. (1) requires the calculation of the scattering cross section of the scattered wave field by a single spherical air void. The scattering cross section is defined as the equivalent area of a scatterer, and is larger than the physical area of the scatterer—it is the ratio of the scattered power divided by the intensity of the incident wave. This calculation is a classical problem of wave scattering (associated with the scalar Helmholtz equation) and has been addressed by several researchers. This research follows [22] and a detailed analysis is given in Appendix A; the scattering cross section of a longitudinal wave scattering by a spherical void is

$$\gamma^{\mathrm{sca}} = -\frac{4\pi}{\mathrm{Re}(k)} \, \mathrm{Im}\left(-\sum_{m=0} i^m A_m\right). \tag{2}$$

Using Eqs. (1) and (2), numerical calculations are carried out for the longitudinal wave scattering by a spherical void in a viscoelastic cement paste matrix in terms of the normalized wave numbers, ka. For a viscoelastic cement paste matrix, $k = \omega(1/c_L - i\alpha_a/2\pi f)$. Note that the quantity $\alpha_a/2\pi f$ is simply the slope of the attenuation (in Neper per meter) versus frequency function (in Hz) curve obtained from attenuation measurements made in a specimen that consists of viscoelastic cement paste matrix only. Details on the measurement of the viscoelastic properties of the cement paste matrix are provided in Section 4.1.

Fig. 3 shows the normalized scattering cross section $\gamma^{\mathrm{sca}}/\pi a^2$ for an incident longitudinal wave in a cement paste matrix with entrained air voids specimen calculated with Eq. (2), as a function of normalized frequency, ka. Note that if the entrained air void radius, a, is taken to be 0.3 mm, the ka range in Fig. 3 corresponds to a frequency range from DC up to approximately 10 MHz. Fig. 3 clearly demonstrates that the scattering effect is relatively small in the low frequency range, and then it grows substantially before eventually flattening out as the frequency increases. The influence of matrix viscoelasticity on the scattering cross section is also illustrated in the same figure. There is little difference between the elastic and viscolelastic matrix results, with the viscoelasticity mainly affecting the low frequency results. Overall, a viscoelastic matrix results in a larger scattering cross section in the $ka < 1$ range and a smaller scattering cross section in the $ka > 1$ range.

The total frequency dependent attenuation coefficient, α, calculated with Eq. (1) is shown in Figs. 4 and 5 for an incident longitudinal wave as a function of absolute frequency, for a number of different void fractions, ϕ,
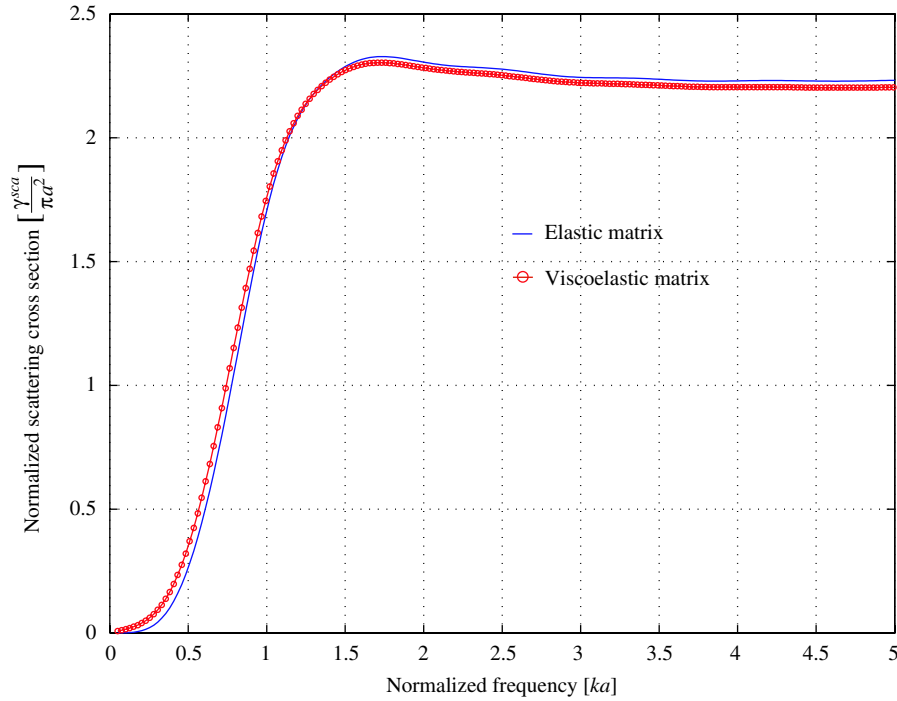

Fig. 2. Schematic of a representative material volume, V.

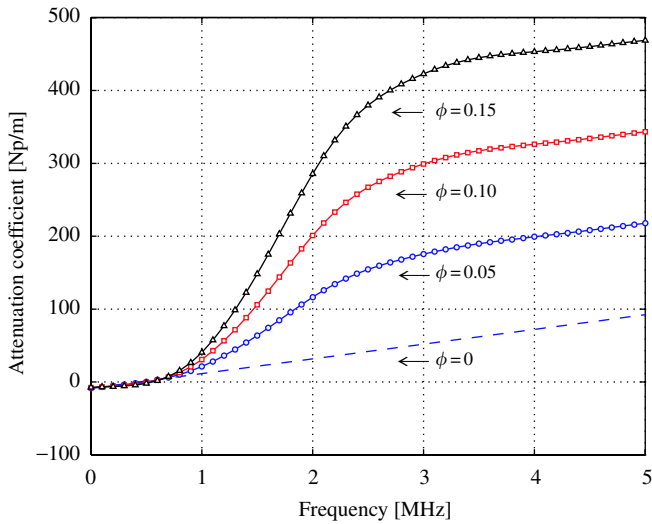Fig. 3. Normalized scattering cross section as a function of normalized frequency.

Fig. 4. Total attenuation, α, versus frequency for different void fractions, ϕ and void radius fixed ($a = 0.3$ mm).
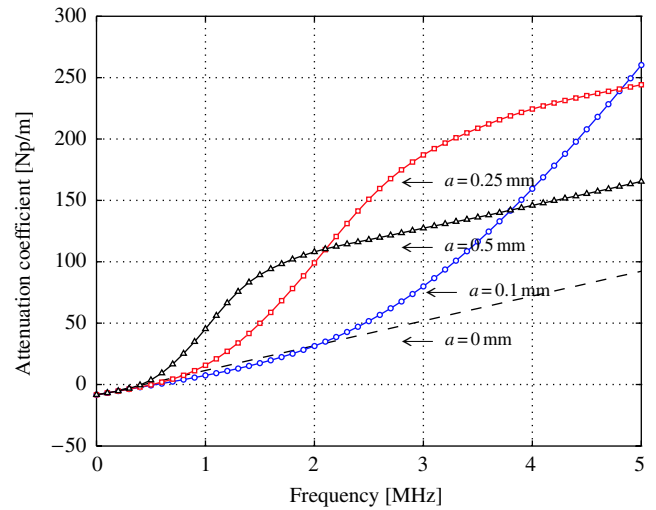

Fig. 5. Total attenuation, α, versus frequency for different void radii, a and void fraction fixed ($\phi = 5\%$).

and void radii, a. The experimentally measured absorption attenuation of the cement paste matrix (see Section 4.1) is presented as a dashed line in both figures to indicate the relative contribution of each of the two loss mechanisms—absorption and scattering. These figures show the influence of the two entrained air void characteristics, void fraction and void radius, and will be used as the "forward problem" results for the proposed inversion scheme. It can be seen that the total attenuation is directly related to the entrained air void size and volume through this frequency range, and

these figures indicate that it should be possible to extract quantitative information about the entrained air void size and distribution in real cement paste specimens.

3. Experimental procedure

Two $10\,\text{cm} \times 20\,\text{cm}$ hardened cement paste cylindrical specimens were cast from commercially available Type I Portland cement and water at a water-to-cement mass ratio of 0.4 in a Hobart mixer. A chemical air-entraining agent
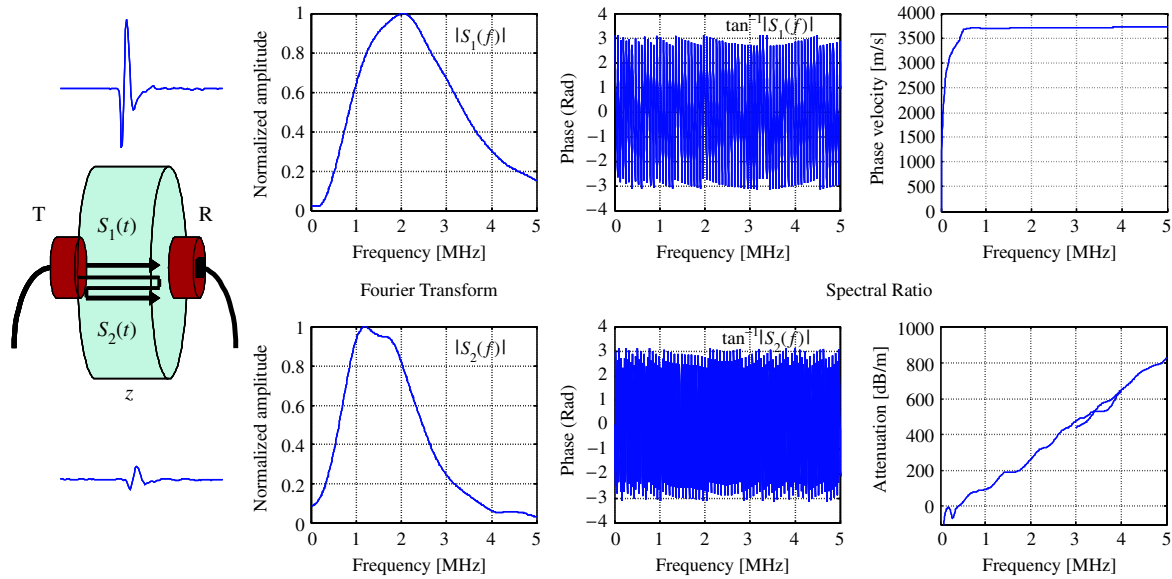
Fig. 6. Attenuation and phase velocity measurement using the spectral ratio technique.

(Darex supplied by W.R. Grace) was added to one of the specimens at about 0.2 percent of the cement by mass during the process of mixing without adjustment of the total volume to produce entrained air voids in the hardened cement paste specimen. This is similar to the procedure by Kalliopi and Philip [23]. Immediately after the completion of mixing and molding, both specimens were covered with plastic caps and kept in moist, sealed plastic containers for 24 h. After 24 h, the specimens were demolded and were stored in sealed plastic containers in an environmentally controlled room for 27 more days at 22 °C. At 28 days of age, they were removed from the room, and were cut using a diamond saw and polished to provide a 25 mm section parallel finished surface. Those specimens found to be most free of visible cracks were selected for the ultrasonic measurements. Fig. 1 shows magnified digital images of typical areas for each of the two specimens (the specimen manufactured without the air-entraining agent is identified as the cement paste specimen, while the specimen manufactured with the air-entraining agent is identified as the entrained air specimen).

Commercial contact transducer pairs (1, 2, and 5 MHz nominal frequencies, Panametrics Inc.) are used along with a Panametrics 5072PR pulser–receiver to transmit long-itudinal (or transverse) ultrasonic waves into each of these specimens. The electrical signal is first amplified with a maximum of 45 dB with a power amplifier. The transmit-ting transducer (T) then converts the electrical signal to a pressure wave. The pressure wave propagates through a specimen and is received by another transducer (R) and converted into the electrical signal. The signal is acquired with a sampling rate of 50 mega samples per second, and with 8-bit resolution with a digital oscilloscope. The signal-to-noise ratio (SNR) is increased by averaging over a large number of signals (i.e., 500). The spectrum of each received signal is calculated using a fast Fourier transform (FFT)

procedure. Spectral ratio analysis [24] is used to measure attenuation and phase velocity; this technique compares the amplitude and phase spectra of two signals recorded on the same specimen which have traveled along two different paths, and is summarized in Fig. 6.

As shown in Fig. 6, the first signal, $S_1(t)$, propagates through one thickness of the specimen (direct longitudinal or transverse wave), while the second signal, $S_2(t)$, propagates through three thicknesses of the same specimen after reflections on both specimen sides. With a pair of finite circular transducers, the amplitude spectra of the two signals are

$$S_1(f) = D(s = z)S_0(f)e^{-\alpha(f)z}e^{i[\omega t - k(f)z + \phi_0]},$$
$$S_2(f) = D(s = 3z)S_0(f)e^{-\alpha(f)3z}e^{i[\omega t - k(f)3z + \phi_0 + \delta\phi]}, \quad (3)$$

where $\alpha(f)$ denotes the total attenuation coefficient, $D(s)$ is the diffraction coefficient proposed by Rogers and Van Buren [25] with $s = 2\pi z/ka^2$, $k(f) = 2\pi f/v(f)$ with $v(f)$ the phase velocity, z is the thickness of the specimen, $S_0(f)$ and $\phi_0(f)$ are the source spectrum and the source phase for $z = 0$, and $\delta\phi$ is the phase shift between the time base of the first and second signal. Thus the corresponding expressions for the attenuation and the phase velocity are

$$\alpha(f) = \frac{1}{2z}[\ln\left(\frac{S_1}{S_2}\right) - \ln\left(\frac{D(s = z)}{D(s = 3z)}\right)],$$
$$v(f) = \frac{(4\pi fz)}{\arg\left(\frac{S_1}{S_2}\right) + \delta\phi}, \quad (4)$$

where arg(·) designates the argument of the complex number under consideration. One can see from Eqs. (3) and (4) that the effect of geometric divergence (the change in the amplitude due to the diffraction effects) is needed when computing attenuation coefficients. The

phase velocity, on the other hand, is not altered by this geometric divergence.

The robustness and accuracy of the proposed experimental procedure is demonstrated by making a set of measurements on a benchmark material, Lucite (polymethylmethacrylate). The measured values are a longitudinal wave phase velocity of 2782 m/s and an attenuation per wavelength of 0.045 Np (1 Neper = 8.686 dB), which can be compared to the published values of 2690 m/s and 0.022 Np [26], and 2750 m/s and 0.041 Np [27]. There is some variability in the published values (especially for attenuation), but the results obtained with the proposed procedure are well within this range.

4. Experimental results

4.1. Cement paste specimen results

Figs. 7 and 8 show the experimentally measured phase velocity, v, and attenuation, α (in Neper/m) as a function of frequency in the cement paste specimen for both longitudinal and transverse waves. Note that the dramatic drop in phase velocity for frequencies below 500 kHz is most likely an artifact of the frequency response of the measurement system; there is insufficient energy in this frequency range, so the spectral ratio analysis may produce spurious values. Only weak dispersion is observed in the frequency range of interest (500 kHz–5 MHz), and both phase velocities are well approximated as a frequency-independent constant (in this frequency range). It is also clear that the attenuation coefficients can be approximated as first-order (linear) equations of frequency (in this range). Note that this linear dependence on frequency for absorption attenuation (the only attenuation mechanism present in these specimens in this frequency range) has been observed in polymers [26], and is referred to as hysteresis absorption. Hysteresis absorption (as well as relaxation and creep) is present in other viscoelastic materials such as
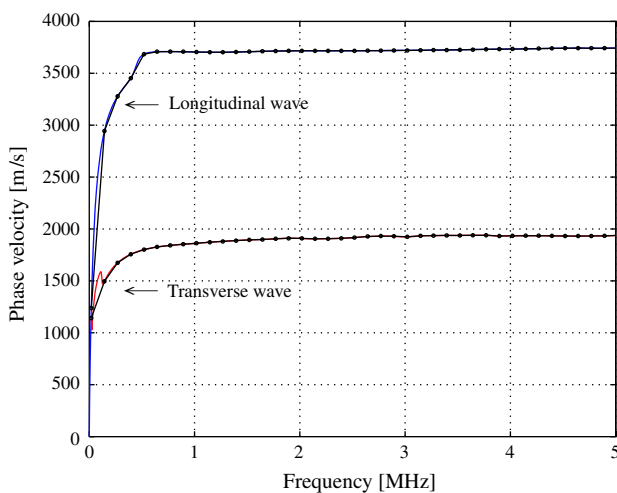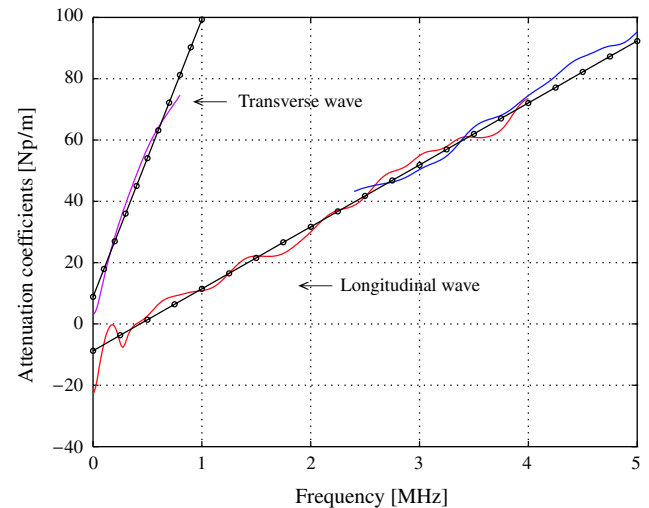

Fig. 8. Frequency dependent attenuation coefficient, α, of longitudinal and transverse waves in the cement paste specimen.

biological tissues [28] and is recognized as occurring in cement-based materials [29]. Relevant material properties of this cement paste specimen (extracted from these experimental measurements) are summarized in Table 1.

4.2. Entrained air specimen results

Fig. 9 shows the experimentally measured attenuation, α (in Np/m) as a function of frequency measured in the entrained air specimen (longitudinal waves only) and compares it to the experimentally measured cement paste results of Fig. 8. Noting from Eq. (1) that the total attenuation in this entrained air specimen is the sum of both absorption (cement paste matrix) and scattering (entrained air voids), it becomes clear that the additional attenuation present in the entrained air specimen is only due to scattering from the entrained air voids. It should be possible to separate these two effects (the scattering effect from the absorption effect) by subtracting the (longitudinal) attenuation measured in the cement paste specimen from the attenuation measured in the entrained air specimen—this result is presented in Fig. 10. This scattering only attenuation will be used in the proposed inversion analysis to obtain quantitative information about the entrained air void size and volume fraction that exist in this specimen.

5. The inverse problem

Section 2 examined the forward problem—application of a single scattering model to determine the attenuation coefficient when the size and volume fraction of the entrained air voids are assumed to be known. The more important problem is the opposite—determination of the entrained air void fraction and size using a set of experimentally measured attenuation coefficients. Ideally, this inverse procedure should also treat the distribution of

Fig. 7. Frequency dependent phase velocity, v, of longitudinal and transverse waves in the cement paste specimen.

Table 1
Material properties of cement paste specimen

Property	Symbol	Value
Longitudinal phase velocity	$c_L[\frac{m}{s}]$	3750
Transverse phase velocity	$c_S[\frac{m}{s}]$	1990
Longitudinal attenuation coefficient; $\alpha_L(\omega) = \alpha_{L0} + \frac{\alpha_{La}\omega}{2\pi}$		
	$\alpha_{L0}[\frac{1}{m}]$	−8.50
	$\alpha_{La}[\frac{1}{m \cdot MHz}]$	20.21
Transverse attenuation coefficient; $\alpha_S(\omega) = \alpha_{S0} + \frac{\alpha_{Sa}\omega}{2\pi}$		
	$\alpha_{S0}[\frac{1}{m}]$	8.85
	$\alpha_{Sa}[\frac{1}{m \cdot MHz}]$	90.46
Poisson's ratio	v	0.26[a]
Young's modulus	$E[\,GPa\,]$	19.5[b]
Density	$\rho[\frac{kg}{m^3}]$	1945[a]
Water-to-cement mass ratio	$\frac{w}{c}$	0.40

[a]Values are calculated from phase velocities.
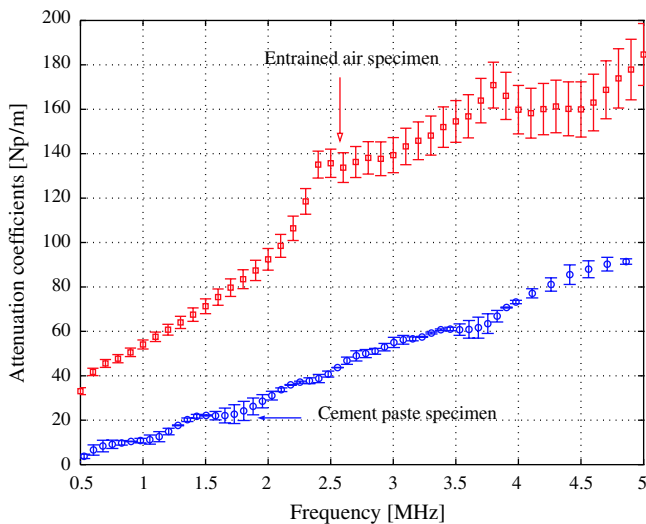[b]Values are taken from Becker et al. [21].

Fig. 9. Comparison of frequency dependent attenuation coefficients, α (longitudinal only) measured in the entrained air and cement paste specimens.

air void sizes as a third unknown, but as a first step, this research assumes that there is only a single size of entrained air voids present within the volume fraction, ϕ.

The Nelder–Mead downhill simplex method [30] is used to predict the entrained air void radius, a, and volume fraction, ϕ, from the experimentally measured attenuation coefficients. This inversion procedure is accomplished by comparing the theoretical results of the attenuation model (which is a function of two variables, a and ϕ) with the experimentally measured attenuation coefficients to determine the best fit between the experimental results and the theoretical prediction. The proposed objective function is $\varepsilon = \sum_f[\alpha(a,\phi)_m - \alpha(a,\phi)_{th}]^2$. The subscript "$m$" denotes that experimentally measured attenuation coefficients, while "th" denotes the values predicted with the theoretical
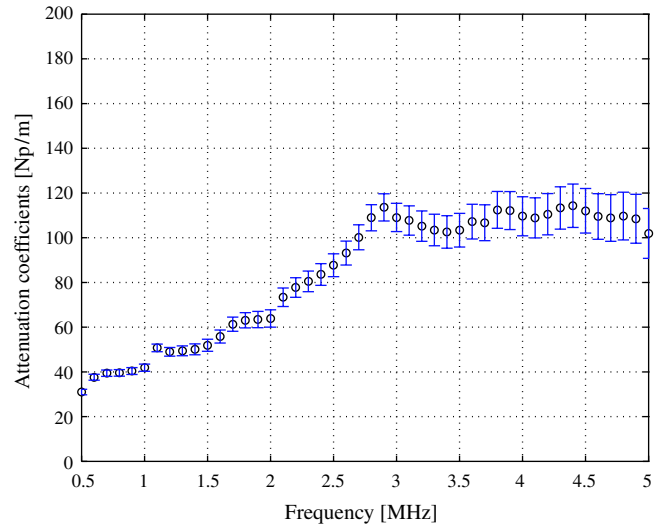

Fig. 10. Scattering portion (only) as a function of frequency (longitudinal waves) in the entrained air specimen.

attenuation model. A flow diagram of the inversion procedure and associated criterion is shown in Fig. 11. The inversion for this particular application is smooth with a direct convergence to a single set of values, and without any local minima; the inversion procedure clearly converges to $a = 0.26$ and $\phi = 3.3\%$ after twenty iterations. Note that these values are within the range measured by Kalliopi et al. [23] for a similar set of specimens.

As a final verification, the values predicted by the inversion procedure ($a = 0.26$ and $\phi = 3.3\%$) are substituted into the theoretical model (Eq. (1)) and the resulting attenuation coefficient (labeled as Forward Prediction ♯ 1) is compared to the experimentally measured values; these results are shown in Fig. 12. There is good agreement between the two data sets, with the best agreement in the 2.25–5 MHz range. There is a greater difference for frequencies below 2.25 MHz. A possible explanation for this difference could be due to the assumption of only a single size of entrained air voids present within the volume fraction, ϕ.

In reality, the air voids in cement paste are not all of the same size, but instead will have a certain statistical distribution. Following Mehta et al. [29], consider a more complicated microstructure system that has two dominant void sizes (each having a normal distribution) as shown in Fig. 13(a). The distribution of the smaller voids (referred to as entrained air voids) has a mean void radius $a = 0.25$ mm, while the second (larger) one (referred to as entrapped air voids) has a mean void radius $a = 1$ mm. Note that both distributions are symmetric, and have the same standard deviation, with more values near the center of their distribution, and relatively fewer in the tails. With this assumed microstructure, the number of voids at a particular radius per unit volume can be calculated by $n_s = 3\phi/4\pi a^3$, which is shown in Fig. 13(b). It is now possible to analytically predict the scattering attenuation coefficient in this microstructure (following [12]) by
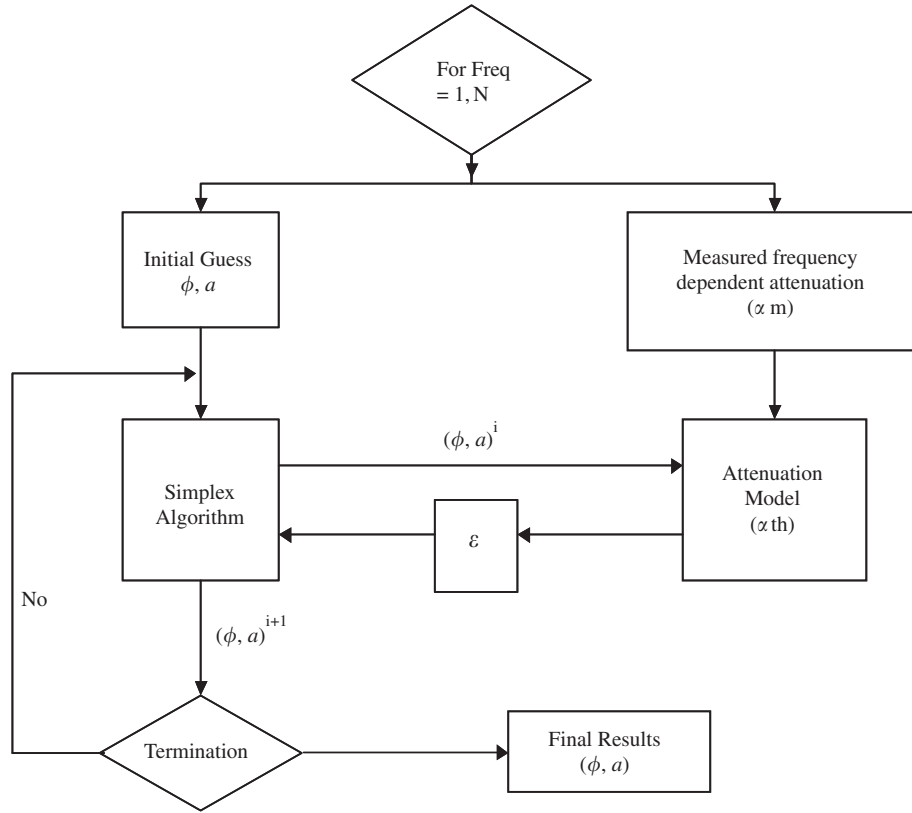
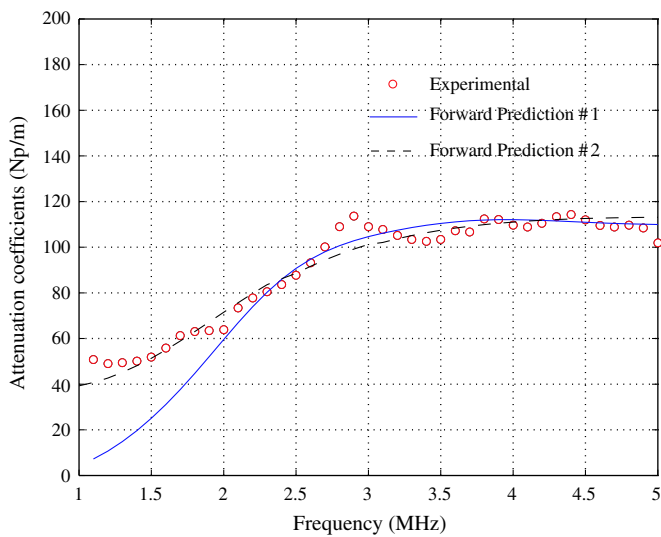Fig. 11. A flow diagram for the inversion procedure.

Fig. 12. Comparison of the experimentally measured attenuation with the forward predictions using simplex optimized values and the assumed normal distributions substituted into the theoretical model.

superimposing these discrete void sizes, and then calculating a new theoretical scattering attenuation with Eq. (1). The theoretical prediction for this new, two-size distribution microstructure is labeled as Forward Prediction ♯ 2 in Fig. 12; it is clear that by assuming the existence of a second (larger but low volume) scatterer, there is a much better agreement between the experimental and theoretical

results. Note that these larger scatterers are most likely present in both the cement paste and entrained air specimens in the form of larger entrapped air voids.

6. Conclusions

This manuscript presents a technique that uses the attenuation of ultrasonic waves to quantitatively characterize the average size and volume fraction of entrained air voids in hardened cement paste. The attenuation and phase velocity of longitudinal and transverse waves in cement paste specimens are predicted by applying established single scattering models to the microstructure of interest. A complementary experimental program measures attenuation coefficients obtained from pulse-burst signals in the frequency range of 500 kHz–5 MHz. An inversion algorithm is then used to determine the average size and the volume fraction of the entrained air voids, and there is good agreement between the model prediction and the experiments in these systems that contained low volume fraction of entrained air voids. It is important to note that the inversion procedure does not account for a distribution of different size air voids, although it is shown that inclusion of a distribution of larger void sizes improves the prediction of scattering attenuation (especially in the frequency below 2.25 MHz). Future work could include this distribution into the inversion algorithm for a more robust technique.
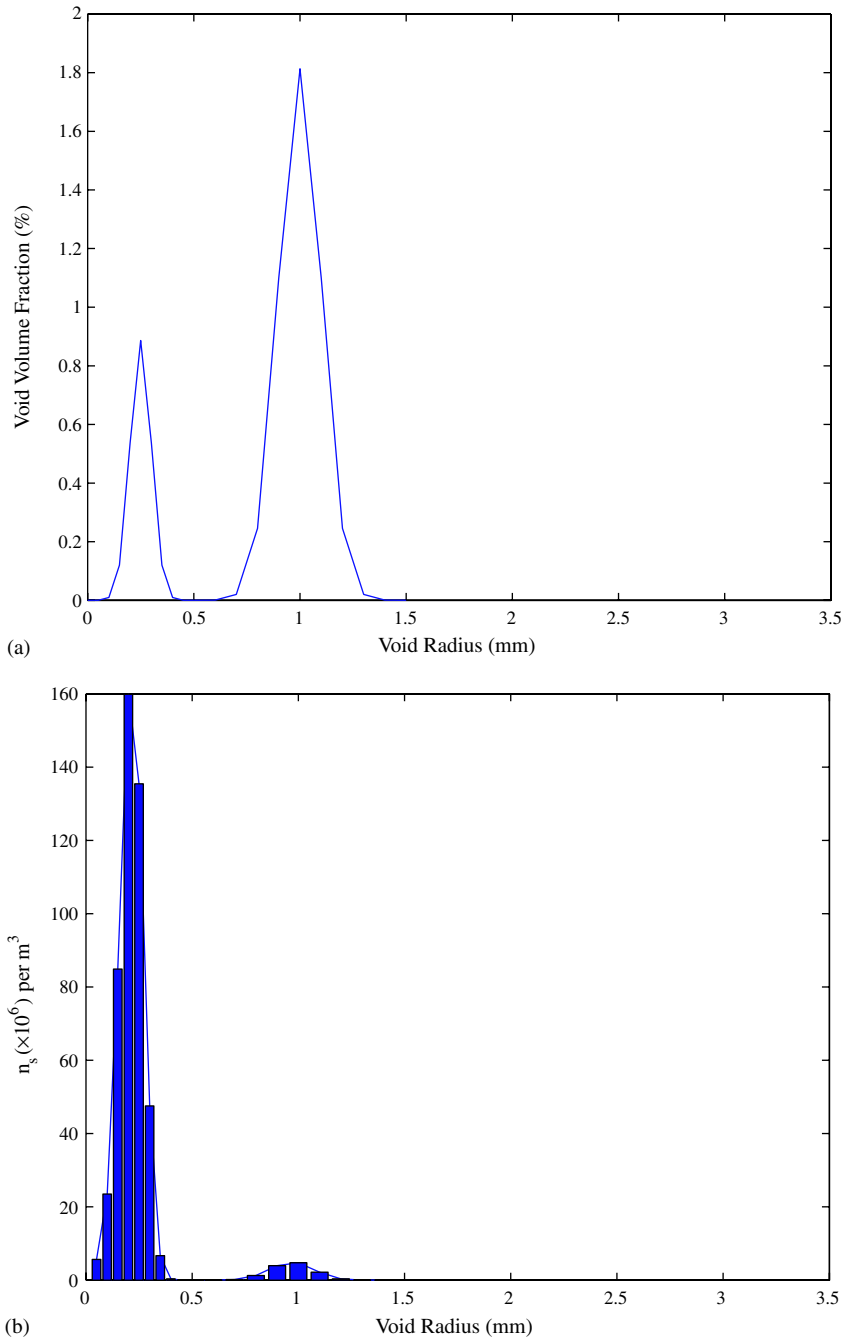
Fig. 13. A plot of (a) percentage of void fraction (normal distribution) (b) number of void density vs. void radius (mm).

Appendix A. Elastic wave scattered by a spherical cavity

For an incident time-harmonic $\langle e^{i\omega t}\rangle$ plane longitudinal wave propagating in the x_1 direction, consider two-dimensional complex displacement potentials, Φ and Ψ, which satisfy the Helmholtz equations, $(\nabla^2 + k^2)\Phi = 0$ and $(\nabla^2 + \kappa^2)\Psi = 0$, with the propagation constants, $k = \omega/c_L - i\alpha_L$ (longitudinal wave) and $\kappa = \omega/c_S - i\alpha_S$ (transverse wave). Using these equations, the problem of a plane longitudinal incident wave encountering a sphere in a viscoelastic solid can be solved using spherical coordinates. The spherical void gives rise to scattered longitudinal and transverse waves outside the sphere (Fig. 14). The solution of the wave equations consists of a series expansion of spherical Bessel functions and spherical
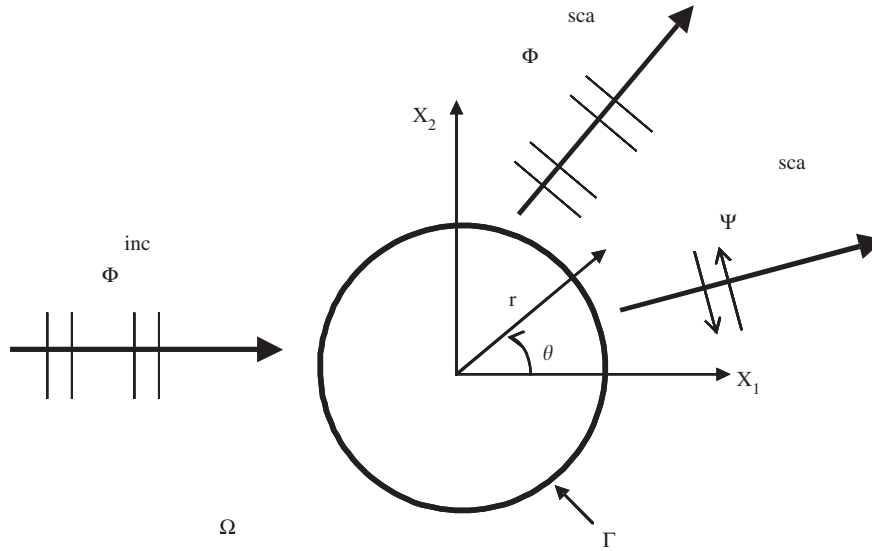
Fig. 14. Single scattering by a spherical cavity.

harmonics with two unknown scattering coefficients (A_m and B_m). These coefficients are then determined numerically from the stress continuity conditions at the void–viscoelastic paste matrix interface (at $r = a$).

Using the stress relations of Ying and Truell [22], the results from two simultaneous algebraic equations are sufficient to determine the two coefficients A_m and B_m. In matrix form, these equations are:

$$\begin{pmatrix} H_{11} & H_{12} \\ H_{21} & H_{22} \end{pmatrix} \begin{pmatrix} A_m \\ B_m \end{pmatrix} = \frac{-1}{k}(-i)^{m+1}(2m+1)\begin{pmatrix} J_{11} \\ J_{21} \end{pmatrix}, \tag{A.1}$$

where

$$H_{11} = -(m^2 - m - \frac{(\kappa a)^2}{2})h_m(ka) - 2(ka)h_{m+1}(ka),$$

$$H_{12} = m(m+1)[(m-1)h_m(\kappa a) - (\kappa a)h_{m+1}(\kappa a)],$$

$$H_{21} = (m-1)h_m(ka) - (ka)h_{m+1}(ka),$$

$$H_{22} = -(m^2 - 1 - \frac{(\kappa a)^2}{2})h_m(\kappa a) - (\kappa a)h_{m+1}(\kappa a),$$

$$J_{11} = -(m^2 - m - \frac{(\kappa a)^2}{2})j_m(ka) - 2(ka)j_{m+1}(ka),$$

$$J_{21} = (m-1)j_m(ka) - (ka)j_{m+1}(ka). \tag{A.2}$$

In these equations, $j_m(\xi)$ and $h_m(\xi)$ are the spherical Bessel function of the first and the third kind, respectively.

The scattering cross section of the spherical void γ^{sca} is related to the finite sums of the expansion coefficients following [11] as

$$\gamma^{sca} = -\frac{4\pi}{Re(k)} \, Im\left(-\sum_{m=0} i^m A_m\right). \tag{A.3}$$

References

[1] Du L, Folliard KJ. Mechanisms of air entrainedment in concrete. J Cem Concr Res 2005;35:1463–71.

[2] ASTM C138, Standard test method for unit weight, yield, and air content (gravimetric) of concrete. Philadelphia, PA: American Society of Testing and Materials; 1992.

[3] ASTM C173, Air content of freshly mixed concrete by the volumetric method. Philadelphia, PA: American Society of Testing and Materials; 1994.

[4] ASTM C231, Standard test method for air content of freshly mixed concrete by the pressure method. Philadelphia, PA: American Society of Testing and Materials; 1991.

[5] Evans AG, Tittmann BR, Ahlberg L, Khuri-Yakub BT, Kino GS. Ultrasonic attenuation in ceramics. J Appl Phys 1978;49:2669–79.

[6] Papadakis EP. Ultrasonic attenuation caused by scattering in polycrystalline metals. J Acoust Soc Am 1965;37:711–7.

[7] Ishimaru A. Wave propagation and scattering in random media. New York: Academic Press; 1978.

[8] Twersky V. Acoustic bulk parameters in distribution of pair correlated scatterers. J Acoust Soc Am 1987;81:1609–18.

[9] Berryman JG. Scattering by a spherical inhomogeneity in a fluid-saturated porous medium. J Math Phys 1985;26:1408–19.

[10] Gaunaud GC, Überall H. Theory of resonant scattering from spherical cavities in elastic and viscoelastic media. J Acoust Soc Am 1978;63:1699–712.

[11] Waterman PC, Truell R. Multiple scattering of waves. J Math Phys 1961;2:512–37.

[12] Sayers CM, Smith RL. The propagation of ultrasound in porous media. J Ultrason 1982;20:201–5.

[13] Morochnik VS. Wave scattering by a spherical inclusion in viscoelastic media. Izvestiya Phys Solid Earth 1987;23:159–61.

[14] Beltzer AI, Brauner N. Wave propagation in random particulate composites: a modification of the Foldy-Lax theory. Acoustica 1988;65:156–62.

[15] Biwa S. Independent scattering and wave attenuation in viscoelastic composites. Mech Mater 2001;33:635–47.

[16] Kim J-YF. Extinction of elastic wave energy due to scattering in a viscoelastic medium. Int J Solids Struct 2003;40:4319–29.

[17] Landis EN, Shah SP. Frequency-dependent stress wave attenuation in cement-based materials. J Eng Mechs 1995;121:737–43.

[18] Popovics S, Bilgutay N, Karaoguz M, Akgul T. High frequency ultrasound technique for testing concrete. ACI Mat J 2000;97:58–65.

[19] Jacobs LJ, Owino J. Effect of aggregate size on attenuation of Rayleigh surface waves in cement-based materials. J Eng Mechs 2000;126:1124–30.

[20] Anugonda P, Wiehn JS, Turner JA. Diffusion of ultrasound in concrete. J Ultrason 2001;39:429–35.

[21] Becker J, Jacobs LJ, Qu J. Characterization of cement-based materials using diffuse ultrasound. J Eng Mechs 2003;39:1478–84.

[22] Ying CF, Truell R. Scattering of a plane longitudinal wave by a spherical obstacle in an isotropically elastic solid. J Appl Phys 1956;27:1086–97.

[23] Kalliopi KA, Philip DC. Air content and size distribution of air voids in hardened cement pastes using the section-analysis method. J Cem Concr Res 1999;29:273–80.

[24] Sears FM, Bonner BP. Ultrasonic attenuation by spectral ratios utilizing signal processing techniques. IEEE Trans Geos Rem Sens 1981;2:95–9.

[25] Rogers PH, Van Buren AL. An exact expression for the Lommel diffraction correction integral. J Acoust Soc Am 1974;55:724–8.

[26] Hartmann B, Jarzynski J. Ultrasonic hysteresis absorption in polymers. J Appl Phys 1972;43:4304–12.

[27] Cheeke JDN. Fundamentals and applications of ultrasonic waves. Boca Raton: CRC Press; 2002.

[28] Fung YC. A first course in continuum mechanics, third ed. NJ: Prentice-Hall; 1993.

[29] Mehta PK, Monteiro PJM. Concrete: microstructure, properties, and materials, third ed. New York: McGraw Hall; 2006.

[30] Nelder JA, Mead R. A simplex method for function minimization. Comp J 1965;7:308–13.